Earth and Planetary Science Letters 297 (2010) 435–445

Contents lists available at ScienceDirect

Earth and Planetary Science Letters

journal homepage: www.elsevier.com/locate/epsl

Complex subduction and small-scale convection revealed by body-wave tomography of the western United States upper mantle

Brandon Schmandt *, Eugene Humphreys

Department of Geological Sciences, University of Oregon, Eugene, OR 97403, USA

ARTICLE INFO

Article history:
Received 15 April 2010
Received in revised form 21 June 2010
Accepted 24 June 2010
Available online 16 July 2010

Editor: R.W. Carlson

Keywords:
upper mantle
tomography
subduction
small-scale convection

ABSTRACT

New high-resolution P- and S-wave tomography of the United States upper mantle from the Pacific Coast to the Great Plains reveals strong multi-scale heterogeneity closely correlated with tectonic and magmatic activity. We invert teleseismic travel-time residuals from the EarthScope Transportable Array and more than 1700 additional temporary and permanent stations for 3-D velocity perturbations to a depth of 1000 km. The inversion uses recent advances in western U.S. crust models to better isolate the mantle component of travel-time residuals, and frequency-dependent 3-D sensitivity kernels to map travel-time residuals, measured in multiple frequency bands, into velocity structure. In addition to separate V_P and V_S models, we jointly invert the two datasets for V_P/V_S perturbations by imposing a smoothness constraint on the $\delta ln V_S/\delta ln V_P$ field. The joint inversion helps us identify regions where partial melt is probable. The amplitude of V_P, V_S, and V_P/V_S variations is greatest in the upper 200 km of the mantle and the form of velocity anomalies suggests a provincially heterogeneous lithosphere and the occurrence of widespread small-scale convection. Partially molten mantle is inferred beneath Yellowstone and the eastern Snake River Plain (SRP), the Salton Trough, and the Clear Lake volcanic field. The inferred depth extent of partial melt is consistent with a generally hydrated upper mantle and elevated temperatures beneath the eastern SRP and Yellowstone. Despite continuous subduction since the Cretaceous, the distribution of sub-lithospheric high-velocity anomalies is dissected (similar to other recent studies). Based on our new tomography models, western U.S. geologic history, and plate–tectonic reconstructions, we infer patchy and incomplete removal of the flat-subducting Laramide slab and slab tearing associated with Eocene accretion in the northwestern U.S.

© 2010 Elsevier B.V. All rights reserved.

1. Introduction

The western United States provides an excellent region for advancing our understanding of mantle heterogeneity caused by subduction (Sigloch et al., 2008), small-scale convection of the lithosphere (Bird, 1979; Zandt et al., 2004), and plumes (Schutt and Dueker, 2008; Smith et al., 2009) both because these processes appear to be active there and because the seismic data are unparalleled. In particular, the transportable array (TA) component of EarthScope's USArray is providing a fundamental advance in data coverage, allowing for continuous high-resolution imaging from the Pacific coast to the western Great Plains. Seismologists have long recognized that subduction beneath western U.S. occurs into an anomalously low-velocity upper mantle (Romanowicz, 1979; Grand, 1994); on average, mantle seismic velocities between 100 and 200 km depth are among the lowest on Earth (Lebedev and van der Hilst, 2008). Imaged within this generally low-velocity mantle are small-scale high-velocity structures that exhibit seismic contrasts as great as that observed between average craton and the tectonically active western U.S. (Humphreys and Dueker, 1994). That the western U.S. upper mantle is vigorously active is implicated by geologic study, which has shown that the western third of the U.S. is undergoing post-Laramide orogenic collapse with accompanying volcanism (Coney and Harms, 1984; Burchfiel et al., 1992), and it has been uplifted into one of Earth's great plateaus. The elevated western U.S. interior is comprised of distinctive tectonic and geomorphic provinces (Fig. 1), including the highly extended and magmatically altered Basin and Range, the Laramide-contracted and unextended Colorado Plateau and Rocky Mountains, and the tilted and intact Great Plains. It appears that large portions of the Great Plains, Rocky Mountains and Colorado Plateau have been uplifted in part since the Laramide orogeny (Heller et al., 2003), with evidence for uplift continuing to the present (Riihimaki et al., 2007; Karlstrom et al., 2008). This indicates young and ongoing mass redistribution at depth.

Ongoing transition of the westernmost North America plate margin from subduction to transform (Atwater, 1970) has been used to predict a triangular slab-free area beneath most of the Basin and Range and southern Rocky Mountains (Dickinson and Snyder, 1979), although geologic evidence for complex subduction since ~80 Ma suggests that the actual slab distribution may be more complicated

* Corresponding author.
E-mail address: bschmand@uoregon.edu (B. Schmandt).

0012-821X/$ – see front matter © 2010 Elsevier B.V. All rights reserved.
doi:10.1016/j.epsl.2010.06.047

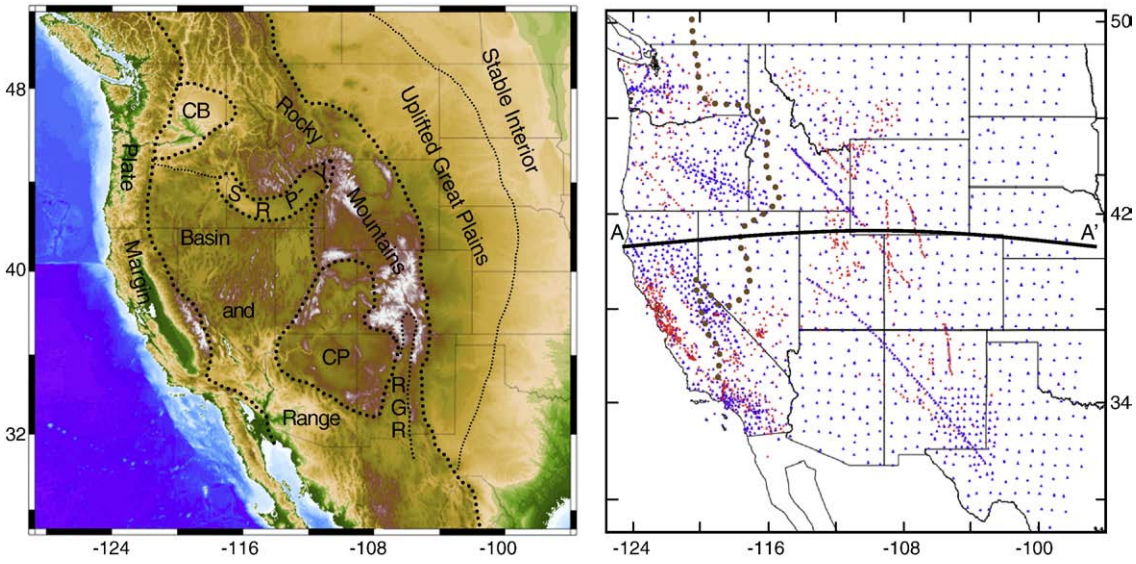

Fig. 1. Regional geography and station map. Major geologic provinces of the western U.S. are labeled on the left map abbreviated names include the Columbia Basin (CB), Snake River Plain–Yellowstone hotspot track (SRP–Y), Colorado Plateau (CP), and Rio Grande Rift. The right map shows the stations used only for P data (red) and stations used for both P and S data (blue). We include TA data up to December 2009. The 0.706 Sr line (brown dotted) indicates the approximate boundary between accreted oceanic terranes to the west and Precambrian North America to the east (from DeCelles, 2004). The location of cross-section A–A′ used for the synthetic test results in Fig. 3 is indicated.

than that predicted by plate kinematics. In particular, the distribution of Laramide thrust faulting and magmatism suggests flat-slab subduction as far inboard as the Rocky Mountain Front (Bird, 1984), and the subsequent ignimbrite flare-up of the Basin and Range is thought to represent slab removal (Coney and Reynolds, 1977) beneath the Basin and Range (Humphreys, 1995). Accretion of the Siletzia ocean lithosphere ~50 Ma in the northwestern U.S. necessitated slab tearing and initiation of subduction at Cascadia (Humphreys, 2009). The fate and distribution of ~5000 km of slab subducted since 80 Ma is the subject of several recent seismic investigations (Sigloch et al., 2008; Burdick et al., 2009; Roth et al., 2008, Tian et al., 2009, Xue and Allen, in press).

In this paper we present new travel-time tomography models of 3-D V_P, V_S, and V_P/V_S perturbations in the western U.S. upper mantle. Use of nearly all available teleseismic body-wave data and recently advanced crustal models results in upper mantle resolution superior to previous efforts, and imaging of V_P/V_S perturbations helps identify where properties other than temperature have a strong influence on seismic structure.

2. Data and methodology

2.1. Travel-time data

We use relative travel-time residuals of teleseismic P and S phases observed at 2661 seismic stations (1648 stations for S) in the western U.S. to invert for 3-D perturbations in upper mantle V_P, V_S, and V_P/V_S (Fig. 1). Direct P and PKP phases observed on the vertical component are used for P-wave residuals. S-wave data are rotated to radial and tangential components and residuals are measured for direct S observed on the tangential component and SKS observed on the radial component. Residual times are measured by cross-correlation of band-pass-filtered waveforms in up to four Gaussian frequency bands with center frequencies of 1, 0.5, 0.3, and 0.1 Hz for P-waves and 0.4, 0.1, and 0.05 Hz for S-waves. Data from short-period stations are only used for 1 Hz P residuals. In total, we use 248,000 P residuals (47% 1 Hz, 26% 0.5 Hz, 22% 0.3 Hz, and 5% 0.1 Hz) and 84,000 S residuals (6% 0.4 Hz, 52% 0.1 Hz, and 42% 0.05 Hz). We prefer to use more high-frequency data in the inversions because these data sample the mantle over smaller length-scales, there is dense station spacing in the region, and residual time uncertainty increases with period. However, relatively few high quality S arrivals are observed at 0.4 Hz. The root mean square (RMS) values of the P and S residuals are 0.43 s and 1.18 s, respectively. The mean of the travel-time residuals must be zero because we use relative times; consequently, we cannot constrain the mean 1-D velocity structure beneath the western U.S.

We use topography and crustal velocity and thickness models to calculate ray theoretical travel-time corrections for crustal heterogeneity. We expect that frequency-dependence of crust correction times (Ritsema et al., 2009) is small for the phases and frequencies in our relative travel-time dataset. Recent results using TA data constrain variations in crust thickness (Gilbert and Fouch, 2007) and velocity (Yang et al., 2008; Lin et al., 2008) across the western U.S. These results serve as a background model, which is replaced by higher-resolution local models that cover most of California (Tape et al., 2009; Thurber et al., 2009) and the Yellowstone region (Stachnik et al., 2008). For most of the western U.S. only V_S crustal models derived from dispersion of diffusive Rayleigh waves are available (Yang et al., 2008; Lin et al., 2008) and we assume a mean crustal V_P/V_S of 1.74 (Chulick and Mooney, 2002) to calculate correction times for P arrivals. This simple scaling of V_S to V_P will introduce some error, but these errors are small compared to the errors that would be introduced by ignoring strong crustal structures such as basins and crystalline mountain ranges. The respective P and S crust time corrections have RMS values of 0.11 and 0.18 s, with ~65% of the RMS resulting from crust thickness variations. After correction, the RMS of the P and S residuals is 0.41 and 1.15, respectively. That the RMS of the residual times is approximately the same after crust corrections indicates that there is not a simple correlation between the crust structure and integrated travel-time residuals. This observation cautions against relying solely on inversion-based station terms to correct for crust structure, because station terms effectively reduce the magnitude of travel-time residuals and would therefore lead to diminished recovery of mantle heterogeneity.

Linear regression of P and S residuals for common stations and events provides an estimate of ray path integrated $\delta lnV_S/\delta lnV_P$ in the region. The linear fit with a slope of 2.84 minimizes a weighted sum of the squared errors, which accounts for uncertainties in P and S residuals (Fig. 2)

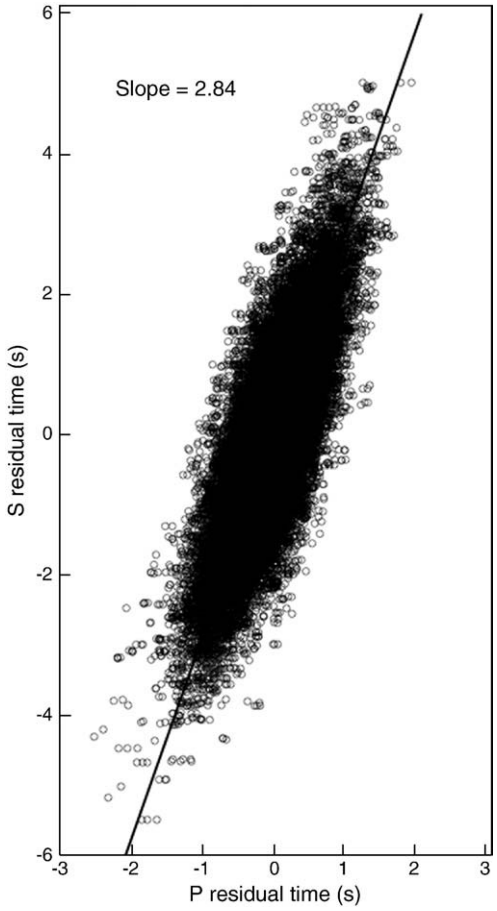

Fig. 2. Linear regression of P and S residuals. We use 56,000 P (62% 0.3 Hz and 38% 0.5 Hz) and S (0.1 Hz) residuals from events with at least 40 common stations to estimate the value of *a*. Typical uncertainties for residual times are ~1/20 of the dominant period. The fit line has a slope of 2.84 with a bootstrap standard error of 0.06.

estimated following VanDecar and Crosson (1990). Using station terms from fewer and more irregularly distributed stations in the western U.S., Romanowicz and Cara (1980) found a slope of 2.54. Our best-fit slope, 2.84, corresponds to $\delta lnV_S/\delta lnV_P$ of 1.57 assuming an average upper mantle V_P/V_S of 1.81 as in AK135 (Kennett et al., 1995). Mantle temperature variations are predicted to produce $\delta lnV_S/\delta lnV_P$ of 1.2–2 (Anderson et al., 1992; Goes et al., 2000) depending primarily on the assumed attenuation structure. To account for the anelastic contribution of temperature variations we assume mean upper mantle Q_S of 100 and negligible bulk attenuation to calculate mean Q_P of 225. The assumed Q values are guided by the Rayleigh-wave attenuation study of Yang and Forsyth (2008) who find mean Q_S of ~95 in the upper 200 km of the southern California mantle, and a recent global study (Dalton et al., 2008) that Q_S beneath the southwest U.S. at ~100 km depth to be lower than the mean for the entire study area. Using these Q values with the scalings of Karato (1993), $\delta lnV_S/\delta lnV_P$ of ~1.6 is expected for thermal variations. Thus, it appears the residual times are consistent with temperature being the dominant cause of velocity variations. However, slope analysis of residual times is expected to underestimate *a*, and consequently $\delta lnV_S/\delta lnV_P$, because the residuals are an integrated sampling of 3-D heterogeneity in the volume about the entire ray path. Furthermore, the mean wavelength of the measured S-waves is ~2 times the mean wavelength of the P-waves so the S residuals average over larger mantle volumes and likely underestimate the magnitude of V_S variations and hence $\delta lnV_S/\delta lnV_P$. To better constrain $\delta lnV_S/\delta lnV_P$ in the presence of 3-D heterogeneity we perform a joint inversion of the P and S datasets (see Section 3.2).

2.2. Tomographic method

We use frequency-dependent 3-D sensitivity kernels to relate travel-time residuals to perturbations of model parameters. We only consider sensitivity in the first Fresnel zone and we use an approximation of the Born theoretical, "banana-doughnut" kernel (Dahlen et al., 2000) within the first Fresnel zone. A detailed description of the method is given in Schmandt and Humphreys (2010).

Nodes at the vertices of an irregular, rectangular 3-D mesh parameterize the model space. The model domain extends from 35 km to 1015 km depth, and the vertical distance between nodes increases gradually from 30 km (at 60–90 km depth) to 65 km (>820 km depth) to address growing first Fresnel-zone width and decreasing resolution. Horizontal node spacing is smallest beneath the interior of the TA (40 km) and gradually increases moving outward with the largest spacing (60 km) beyond the boundary of the entire array, where there is a paucity of crossing rays. Resolution is poor in the 35 km layer as a result of near vertical ray path orientation and uncertainties in the *a priori* crust model. This layer tends to absorb both errors in the crust model and crust and uppermost mantle velocity variations that are not well constrained by our data. In areas with only TA data, good crossing ray coverage is not achieved until ~80 km depth. However, because we use more than 1700 stations in addition to the TA (>700 for S data) there is good crossing ray coverage in the 60 km layer throughout much of the western U.S.

In addition to the V_P and V_S model parameters, we invert for station and event parameters. Because we correct for crust thickness and velocity variations, the station terms are only intended to address local site effects and errors in the *a priori* crust model; consequently, we apply strong station damping to keep the station terms from absorbing mantle structure. The RMS of the station terms is 0.05 s and 0.08 s for P and S, respectively. Event terms represent adjustment of the mean arrival time for the specific set of stations that record each event. These terms are important because we solve for velocity perturbations rather than absolute velocity, and the mean velocity structure varies significantly for different arrays in the western U.S.

We follow the same procedure as Schmandt and Humphreys (2010) for the construction and solution of the inverse problem. In addition to separate V_P and V_S inversions we also jointly invert the P and S datasets for V_P/V_S variations by simultaneously imposing a smoothness constraint on δlnV_S, δlnV_P, and $\delta lnV_S/\delta lnV_P$ fields (similar to Hammond and Toomey, 2003). Thus, deviations from the reference V_P/V_S values of AK135 are not penalized, but roughness is penalized. The P and S datasets are equally weighted in the joint inversion because the main motivations for the joint inversion are to explore the consistency of the two datasets and obtain better estimates of $\delta lnV_S/\delta lnV_P$ in the upper mantle.

2.3. Synthetic resolution tests

Synthetic tests demonstrate expected model resolution with the assumptions of an isotropic elastic mantle, accurate ray locations, and sensitivity limited to the first Fresnel zone. The synthetic structure consists of three checkerboard layers embedded in a neutral background (Fig. 3). In general, the recovery of the input structure in the P and S velocity models is good, although we find some streaking and amplitude loss owing to the sub-vertical orientation of teleseismic rays and the preference for minimum energy structure in the inversion algorithm. Peak P amplitude recovery generally is higher than peak S amplitude recovery, 70–80% and 60–70%, respectively. It also appears that the shorter wavelength P data more accurately recover the input structure near the margins of anomalous volumes. The synthetic test results for V_P/V_S perturbations show little geometric distortion of the input structure, but lower peak amplitude recovery, 50–60%, (Fig. 3), which indicates the inversion under-estimates the magnitude of V_P/V_S heterogeneity more than P and S

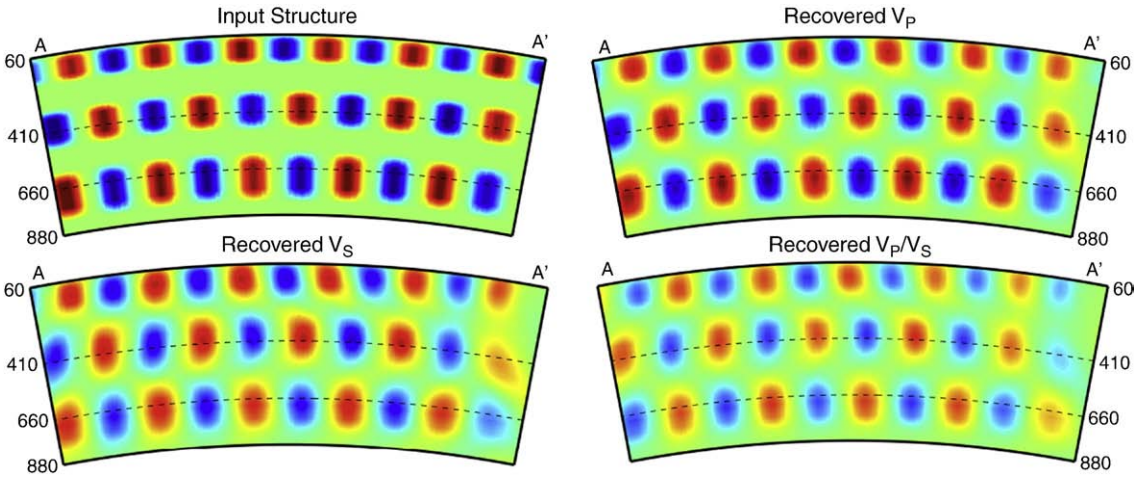

Fig. 3. Synthetic test results. The same cross-section, labeled on Fig. 1 as A–A′, is shown for the input structure (upper left), recovered V_P (upper right), recovered V_S (lower left), and recovered V_P/V_S (lower right). Note that the sign of the input structure should be reversed for the V_P/V_S test, but the geometry of anomalous volumes is the same. Color scale limits for the recovered structure are the respective peak perturbations in the input structure for V_P (±3%), V_S (±5.5%), and V_P/V_S (±2.3%). More images from the synthetic test results are available in the online supplement.

velocity heterogeneity. In general, the P model is expected to have better resolution than the S model as a result of ~1000 more stations, shorter wavelengths of measured P-waves, and the relative abundance of high quality teleseismic P arrivals from regions with lower magnitude and less frequent seismicity (i.e., more useable P arrivals from mid-ocean ridge and transform earthquakes improves ray path distribution). Consequently, we prefer to give the structure resolved by the P data more weight in our interpretations, and hence we present more figures from the P model in the primary manuscript, but a complete set of V_P, V_S, and V_P/V_S images from the separate and joint models is available in the online supplement for comparison.

3. Results and discussion

3.1. Fit to the data

The quality of a least-squares optimal solution to an ill-posed inverse problem is commonly evaluated by the data variance reduction. Because resolution varies widely throughout the model domain and we rely on assumptions known to be invalid (such as isotropy), the overall variance reduction of a tomography model tends to be a misleading and optimistic indicator of quality. The variance reductions of the isolated P and S inversions are 87.3% and 85.6%, respectively, indicating that velocity models produced under the assumptions used can explain nearly all the observed variance in travel-time residuals. A more realistic metric of model quality is obtained by calculating the variance reduction only for portions of the model domain where resolution is greater than some minimum threshold. Each node is assigned a "hit-quality" index, ranging from 0 (for not sampled) to 1 when a node is sampled by at least 5 rays from each back-azimuth quadrant and at least 5 rays from core phases. Our chosen threshold is 0.4 (i.e., several rays from at least 2 back-azimuth quadrants), and we exclude nodes in the top layer (35 km) and bottom two layers (950 and 1015 km). Both the formulation for hit-quality index and selection of the well-resolved threshold are somewhat subjective, and are chosen based on recovery of synthetic test structures (and the simple fact that rays intersecting at high angles are necessary for good resolution). The variance reductions for the overall model and well-sampled portion of the model are given in Table 1 for the isolated P and S inversions and the joint inversion.

Comparing the overall and well-sampled variance reduction provides an approximate metric of how much of the overall residual reduction is accounted for by structure in volumes that are not well-sampled. The decrease in variance reduction from the isolated P and S inversions to the joint P and S inversion also serves to indicate the validity of our modeling assumptions. Discrepancies between the P and S datasets are likely to result from differences in station density, anisotropy as sampled by the orthogonal polarization of P and S teleseismic body-waves, and the difference in frequency bands used to measure the P and S residuals. Differences between the separately inverted P and S models are more prominent at depths greater than ~300 km. At these depths, the jointly inverted P and S models are more similar to each other and to the separately inverted P model. Because the two datasets are equally weighted in the joint inversion this suggests the P data have at least slightly better resolution than the S data. We consider the 66.7% variance reduction in the well-sampled portion of the model from the joint P and S inversion to be the most informative indication of how well the isotropic, elastic tomography models can fit the data.

3.2. Seismic heterogeneity and physical state

The most striking aspect of the tomographic images is the strong multi-scale heterogeneity in the upper 200 km (Fig. 4). The V_P and V_S models are highly mutually consistent, and velocity and V_P/V_S perturbations are generally negatively correlated. Excluding the most anomalous 1% of model parameters, peak-to-peak amplitudes at less than 200 km depth in the well-sampled model space are 7.8% V_P, 14.5% V_S, and 7.2% V_P/V_S. This magnitude of heterogeneity is large relative to other body-wave tomography studies, but is in close agreement with surface-wave tomography studies using TA data (Yang et al., 2008; Pollitz and Snoke, 2010). Physical origins of seismic velocity variations are variations in temperature, partial melt, anisotropy, bulk and volatile composition. Seismic structure of magnitude as great that imaged must include an important contribution from temperature. It is informative to consider the magnitude of temperature variations required if the entire peak-to-peak velocity variations are attributed to temperature change. Using the temperature derivatives of Karato (1993) and the Q values from Section 2.1

Table 1
RMS misfit of P, S and joint P–S models, measured over the entire model and measured over only the well-resolved portion of the model.

	P model		S model		Joint model	
	Entire	resolved	Entire	resolved	Entire	resolved
Individual	87.3%	75.5%	85.6%	72.4%	–	–
Joint	81.1%	71.2%	79.8%	64.9%	80.5%	67.7%

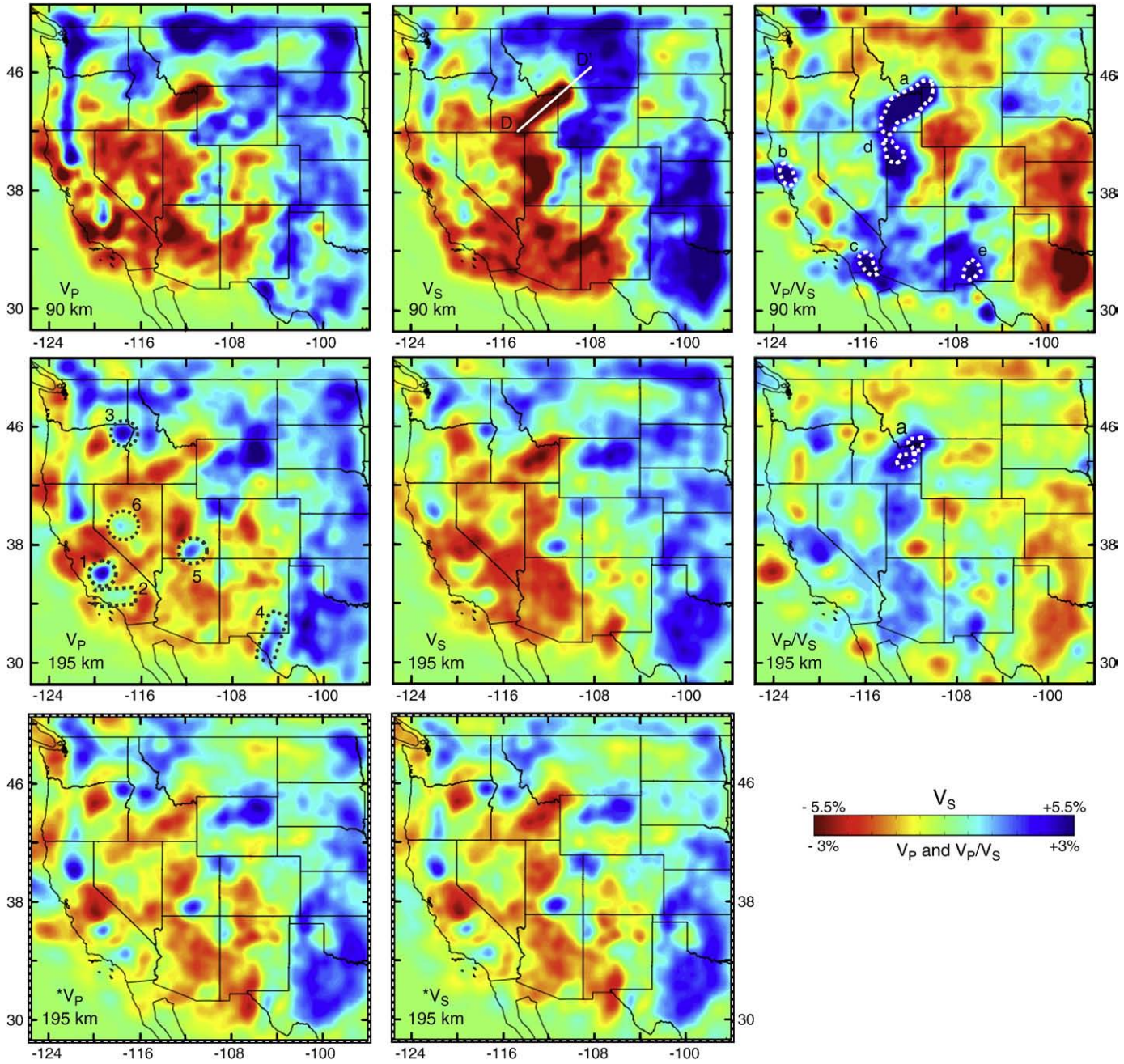

Fig. 4. Shallow upper mantle map slices. Color represents velocity perturbations relative to the mean in each depth layer and that mean is not constrained by our relative travel-time data. Hypothesized lithospheric instabilities are outlined (gray dashed) on the 195 km V_P map in the left column, second row: (1) southern Great Valley (Zandt et al., 2004), (2) Transverse Ranges (Humphreys and Hager, 1990), (3) Wallowa Mountains (Hales et al., 2005), (4) western Great Plains (Song and Helmberger, 2007), (5) Colorado Plateau (Sine et al., 2008), and (6) central Nevada (West et al., 2009). Inferred partial melt regions (Section 3.2) are outlined (white dashed) on the V_P/V_S maps in the right column. The maximum inferred depth of melt is ~195 km beneath (a) Yellowstone and the eastern SRP, and ~125 km for (b) the Salton Trough, (c) Clear Lake volcanic field, (d) northeastern Great Basin, and (e) southern RGR. In the third row are 195 km map slices from the jointly inverted model ($*V_P$,$*V_S$) for comparison with the separately inverted and images in the second row. See Supplemental figures for a complete set of images from the separate and joint inversions. The location of cross-section D–D′ from Fig. 8 is indicated in the top, center panel.

the peak-to-peak V_P and V_S variations correspond to temperature variations of 850 K and 960 K for V_P and V_S, respectively. These values are very high, but perhaps possible given the potential range of lithosphere and asthenosphere temperatures in a model that spans Archean lithosphere, Cenozoic accreted terrains, the highly extended Basin and Range, and the Yellowstone hotspot. Alternatively, a small amount of partial melt in the asthenosphere would reduce the predicted temperature variations to more reasonable values. For example, up to 0.5% partial melt in the asthenosphere would reduce the required temperature variations by ~200 K (Hammond and Humphreys, 2000). The existence of partial melt in the lowest velocity volumes seems likely considering the strong correlation with young volcanic fields and the low mean velocity of the western U.S. asthenosphere (Lebedev and van der Hilst, 2008). Strengthening the idea that non-thermal effects contribute significantly to velocity variations is an awareness that regularized travel-time inversions underestimate the true magnitude of velocity variations leading to even greater estimated temperature variations.

Aside from variations in temperature and partial melt, V_P/V_S anomalies can be caused by lateral variations in bulk and volatile composition.

Two potential compositional influences on mantle V_P/V_S are hydration, whose effects on velocity are relatively modest in the shallow upper mantle where water solubility is low, and melt depletion. Hydration of the western U.S. lithosphere (Humphreys et al., 2003) and asthenosphere (Dixon et al., 2004; Yang and Forsyth, 2008) has been suggested, but lateral variations in hydration are unlikely to account for the 5–6% peak-to-peak V_P/V_S variations commonly imaged in the upper 200 km. Jacobsen et al. (2008) find only 0.3% reduction in V_P/V_S for hydrous forsterite with 0.9 wt.% H_2O at deep upper mantle pressure (12 GPa), and water solubility is much lower at the depths where the greatest V_P/V_S variations are imaged. There is no consensus as to how strongly melt depletion affects V_P/V_S (Lee, 2003; Schutt and Lesher, 2006). Melt depletion is generally thought to lower V_P/V_S at least slightly, but variations in melt depletion alone cannot account for more than a small fraction of the magnitude of V_P/V_S variations we find in the western U.S. upper mantle. In general, we are lead to conclude that lateral variations in temperature and partial melt are the dominant causes of the imaged structure.

Theoretically, relative δlnVs and δlnVp variations can be diagnostic of the presence of partial melt. As mentioned in Section 2.1, $\delta lnV_S/\delta lnV_P$ of 1.6 is predicted for thermal variations, whereas partial melt in the upper mantle is predicted to cause $\delta lnV_S/\delta lnV_P$ values of ~2.2–2.3 (Hammond and Humphreys, 2000). Linear regression of model parameters from the well-sampled portion of the jointly inverted model yields best-fit $\delta lnV_S/\delta lnV_P$ value of 1.8 (Fig. 5). This estimate is greater than that derived from the raw residuals, 1.57. We think the difference is a result of integrated sampling of 3-D heterogeneity where the greatest magnitude of $\delta lnV_S/\delta lnV_P$ variations occurs over only a small fraction of the total ray length. We suggest the $\delta lnV_S/\delta lnV_P$ estimate from the joint inversion is too high to be explained solely by thermal variations and the presence of partial melt in the lowest velocity volumes is more consistent with our results.

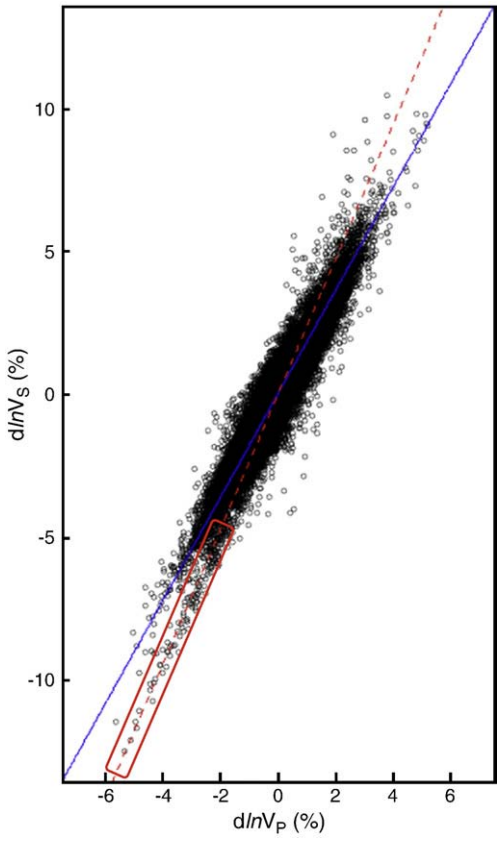

Fig. 5. Upper mantle $\delta lnV_S/\delta lnV_P$ from the joint inversion. Solid blue line indicates the least-squares fit, 1.8 ± 0.05 (bootstrap standard error). The red dashed line indicates the "partial melt trend" (slope of 2.33). Note that many of the very low-velocity model parameters closely follow the partial melt trend. The red rectangle encloses the model nodes where we infer partial melt (nodes <0.3% from the blue fit line are excluded), see Section 3.2 and Fig. 4.

Inspection of the scatter plot of δlnV_S versus δlnV_P model parameters shows that the very low-velocity parameters cluster along two distinct trends rather than being normally distributed about the fit line (Fig. 5). The lower trend is approximately the best-fit value, 1.8. The steeper trend is ~2.33, which is approximately the predicted slope for partial melt, and the lowest velocity points follow this trend remarkably closely. We consider this strong evidence for partial melt in the corresponding mantle volumes. The locations of the model parameters with $\delta lnV_S < -4\%$ that lie within 0.6% of the $\delta lnV_S/\delta lnV_P = 2.33$ "partial melt trend" (but not within 0.3% of the fit line) are outlined on the V_P/V_S tomograms in Fig. 4.

The greatest concentration of model parameters that follow the partial melt trend underlie Yellowstone and the eastern Snake River Plain (SRP) where the inferred prevalence of partial melt decreases rapidly beneath 160 km and disappears deeper than 195 km. We infer decompression induced partial melting to a depth of 90–125 km beneath the Salton Trough and the Clear Lake volcanic field located at the southern edge of the Juan de Fuca-Gorda (JdF-G) slab. Rollback and sinking of the JdF-G slab is thought to drive toroidal flow of oceanic asthenosphere around the slab edge (Zandt and Humphreys, 2008) with an upward poloidal component to direct asthenosphere into the wedge (Piromallo et al., 2006). Mantle ascent beneath the Salton Trough is driven by oblique plate spreading at the northernmost extension of the East Pacific Rise (Stock and Molnar, 1988). Decompression melting beginning at 90–125 km depth is consistent with hydrated peridotite (300–1000 ppm H_2O) ascending along a ridge adiabat (Hirschmann, 2006), and hydration of the western U.S. mantle is likely after more than 100 My of subduction. A maximum melting depth of 160–195 km beneath Yellowstone is consistent with hydrated peridotite (300–1000 ppm H_2O) ascending along a plume adiabat with an excess temperature of 125–225 K (Hirschmann, 2006). Schutt and Dueker (2008), used modeling of Rayleigh-wave velocities to estimate (at 68% confidence) an excess temperature of $\geq$120 K beneath Yellowstone, which would be approximately consistent with initiation of melting at 195 km and 1000 ppm H_2O.

More enigmatic are low-velocity model nodes located beneath the northeastern Great Basin and southern New Mexico that also follow the partial melt trend. In the northeastern Great Basin these nodes correlate with a thin crust and seismic lid (Gilbert and Fouch, 2007; Li et al., 2007); thus, decompression melting of a damp asthenosphere is plausible, but difficult to reconcile with relatively sparse young volcanism compared to the previously mentioned locations. In southern New Mexico there is young volcanic activity and modest mantle ascent is expected to accompany slow Rio Grande Rift (RGR) extension, <0.2 mm/yr (Golombek et al., 1983). However, it is only beneath a small segment of the southern RGR that the P and S model parameters follow the partial melt trend while low-velocity nodes beneath the rest of the RGR do not.

Low-velocity, high V_P/V_S volumes are generally found beneath young volcanic fields, but aside from the specific locations mentioned above we think the depth extent and magnitude of melting are too small to be clearly identified by our body-wave tomography. We suggest the very low-velocity mantle volumes that follow the partial melt trend require melting over a depth range of at least 1 vertical model node distance (30 km) in the well-sampled volume in order to be imaged. The fact that the $\delta lnV_S/\delta lnV_P$ trend of 1.8 for the whole model is steeper than the predicted temperature trend (1.6) suggests that many arrivals to the western U.S. experience some partially molten mantle, most likely over a depth range less than ~30 km thick and shallower than ~60–80 km depth.

Our conclusions regarding upper mantle physical state are generally in agreement with Goes and Van der Lee (2002) who suggest

that large lateral temperature differences owing to variable lithospheric thickness can explain most V_P and V_S variations with ~1% melt locally in the most anomalous regions.

3.3. 3-D seismic structure

Seismic heterogeneity is strongly correlated with major tectonic and magmatic features of the western U.S. Prominent long-wavelength features include high-velocity mantle associated with subduction of the JdF-G slab and beneath the relatively undeformed Colorado Plateau and Great Plains, and generally low-velocity mantle beneath the transform margin, Basin and Range, SRP, and RGR (Fig. 4). Below we discuss salient features of the 3-D V_P, V_S, and V_P/V_S models, and we use knowledge of western U.S. tectonic and magmatic history to make reasoned inferences regarding the geologic origins of anomalous structures.

3.3.1. Evidence for complex subduction

We image a continuous north trending high-velocity slab in the northwestern U.S. upper mantle that must be JdF-G plate subducting beneath the Cascade Arc. The high-velocity slab becomes weak to non-existent beneath northern Oregon at depths greater than ~160 km, whereas the northern and southern portions of the JdF-G slab descend continuously from the trench to depths of ~350 km (Figs. 4 and 6). This defines a slab hole (Roth et al., 2008; Burdick et al., 2009; Tian et al., 2009), which is a robust feature of our P and S tomography models. Assuming a convergence rate of ~4 cm/yr (Gripp and Gordon, 2002), the northern Oregon slab accounts for subduction since only 6–8 Ma, and the segments north and south of the hole account for subduction since ~15 Ma. An abrupt change in subduction geometry at ~15 Ma has also been suggested by geochemical investigation of back-arc volcanism (Carlson and Hart, 1987). The presence of the hole and the separation of the clearly identified JdF-G slab from deeper high-velocity anomalies indicate a complex subduction history. The strongest case for near-continuous subduction is shown in Fig. 7 (A–A′ and B–B′), but north–south continuity of this feature is variable and nowhere greater than ~500 km. Map-view sections within and beneath the transition zone show a general lack of continuity between slab fragments (Fig. 6). Some high-velocity anomalies inferred to be slab fragments beneath the continental interior can be related to western U.S. geologic history. However, a complete accounting of how the large volume of fragmented high-velocity structures relates to the ~5000 km of ocean lithosphere subducted since the Laramide orogeny began (Engebretsen et al., 1985) remains a challenge.

A high-velocity "curtain" extends vertically from near the base of the lithosphere to depths of ~250 km beneath Washington and 500–600 km beneath western Idaho (Figs. 6 and 7). Because the overlying crust experienced considerable Eocene extension, including formation of metamorphic core complexes, and voluminous ignimbritic magmatism (Christiansen and Yeats, 1992) it seems unlikely that this area is underlain by thick, intact ancient lithosphere. We suggest a subducted slab origin for the high-velocity curtain, which roughly follows the inferred early Cenozoic Challis subduction zone on the north and east side of the Columbia embayment (Humphreys, 2009). We interpret the curtain to be Farallon slab that was attached to the leading margin of Siletzia when it accreted ~50 Ma. In order for the slab fragment to persist in this location for ~50 Ma it must be of approximately neutral buoyancy. Plate–tectonic reconstructions have young, 5–30 Ma, lithosphere subducting beneath the Pacific Northwest at this time (Madsen et al., 2006; Muller et al., 2008), hence initial slab buoyancy would have been nearly neutral. Furthermore, portions of the basaltic crust of this slab may have melted in the shallow mantle

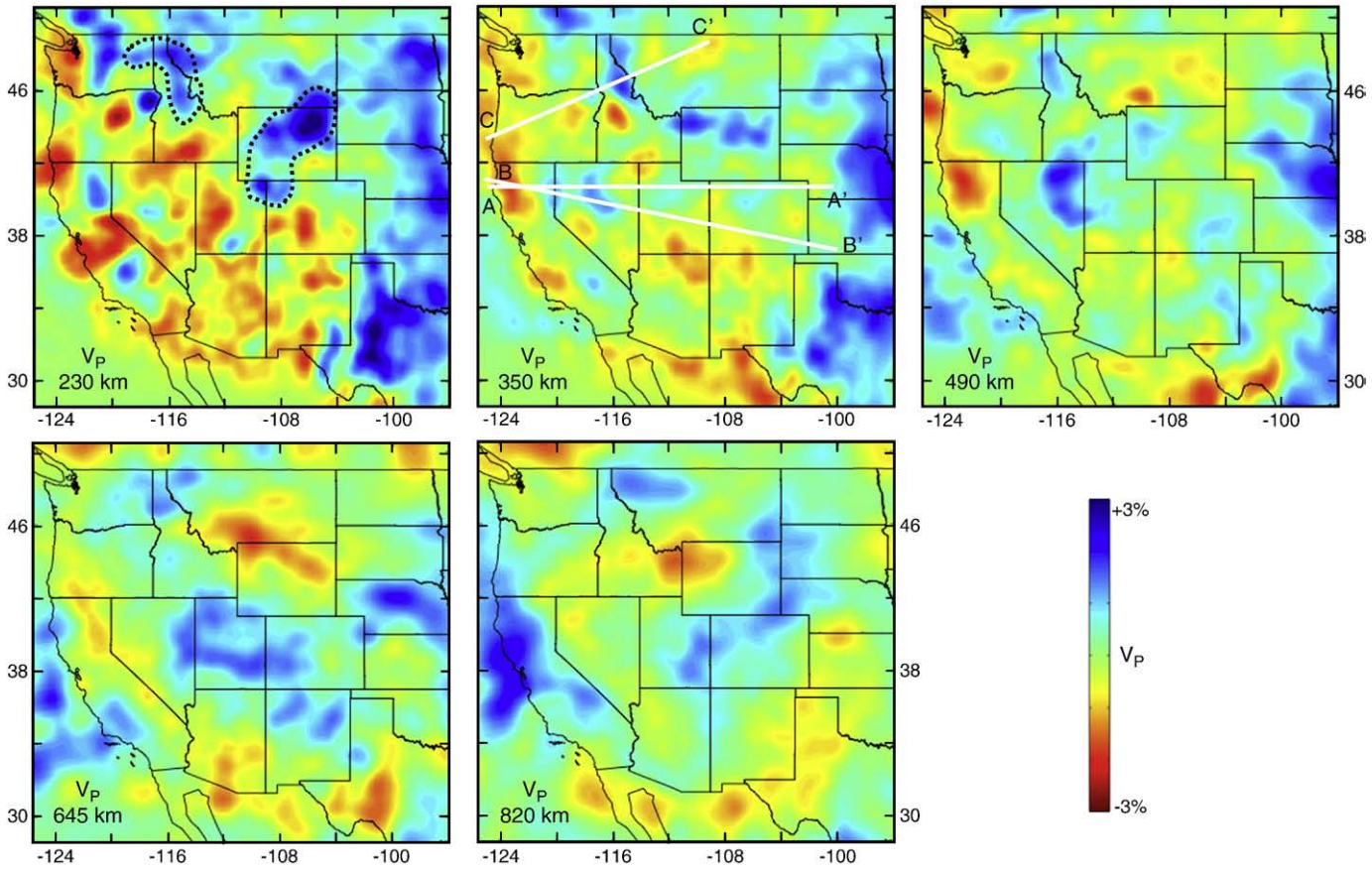

Fig. 6. Deep upper mantle map slices from the V_P model. The slab curtain and thick high-velocity lithosphere beneath the Rocky Mountains discussed in Section 3.3.1 are outlined (black dashed) in the upper left panel. The locations of cross-sections A–A′, B–B′, and C–C′ from Fig. 7 are indicated.

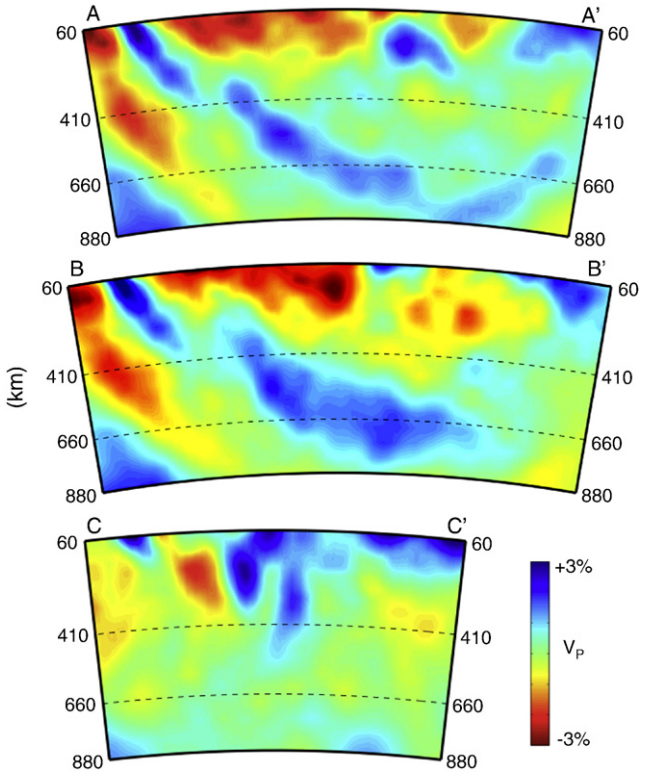

Fig. 7. Cross-sections from the V_P model. The locations of A–A′, B–B′, and C–C′ are shown the map slices in Fig. 6. Section C–C′ crosses the slab hole and slab curtain discussed in Section 3.3.1.

potentially contributing to a ~52–45 Ma episode of voluminous magmatism in Idaho and northern Washington (Gaschnig et al., 2009; Madsen et al., 2006) and avoiding the negative buoyancy of an eclogitic ocean crust.

Regardless of the specific origins of the high-velocity curtain and the hole in the currently subducting JdF-G slab, these structures must fundamentally alter subduction zone mantle flow. Resulting along-strike variations in asthenospheric flow may contribute to dramatic along-strike changes in Cascade Arc volcanism, with widespread and voluminous volcanism in the Oregon Cascades trending to localized and lower-volume volcanism in northern Washington (e.g., Reiners et al., 2002).

Large high-velocity anomalies trending ~SW–NE are found beneath much of Wyoming, northeast Utah, and northwest Colorado, down to ~250–300 km depth (Figs. 4 and 6). It is difficult to explain how ~1.5 km uplift of this area from near sea level at times prior to the Laramide orogeny (inferred from uplift of Cretaceous marine sediments) can be made consistent with a lithosphere thickness as great or greater than that typically found beneath stable cratons (Lebedev and van der Hilst, 2008). An alternative explanation for this structure is that a buoyant ocean plateau (the Shatsky Rise conjugate) inferred to have subducted during the Laramide orogeny (Livicarri et al., 1981; Saleeby, 2003) stalled beneath this region. Subduction of the plateau beneath North America is thought to have caused slab flattening and erosion of basal lithosphere (Spencer, 1996), which may be partly responsible for the uplift of Wyoming. Transfer of the plateau lithosphere from the subducted Farallon to basal North America lithosphere is compatible with the bight in the Farallon slab imaged in the mid-mantle beneath Hudson Bay (Bunge and Grand, 2000). Furthermore, the presence of lateral buoyancy variations in the Farallon slab offers a mechanical explanation for the dissected geometry of the inferred Laramide-age subducted slab and the chaotic distribution of volcanism thought to represent slab flattening (Coney and Reynolds, 1977) and subsequent removal beneath the Rocky Mountains. In order for basal accretion of ocean plateau lithosphere to cause a significant net increase in buoyancy most of its basaltic crust must have been mechanically removed as it traversed the base of the North America lithosphere. If the thick basaltic crust remained entirely intact this explanation for the anomaly does not seem viable because we expect the basalt to convert to dense eclogite.

A strongly anomalous high-velocity body so great in volume that it must be subducted ocean lithosphere extends from ~300 km depth beneath Nevada to ~800 km depth beneath Utah and Colorado (Figs. 6 and 7). Large high-velocity anomalies are also found at 600–900 km depth beneath eastern Wyoming and the Great Plains and are inferred to be subducted slab fragments (Fig. 6). The dismembered structure of these high-velocity anomalies is intriguing considering the rather simple coherent east-dipping structure of the older Farallon slab in the mid-mantle beneath the eastern U.S. (Bunge and Grand, 2000). Plate reconstruction models predict that the highly fragmented slab lies beneath paleo-subduction zones as old as ~75 Ma (Lithgow-Bertelloni and Richards, 1998), i.e., near the beginning of the Laramide orogeny. From these results, we infer patchy and incomplete removal of flat subducting Laramide slab accompanied by slab tearing associated with Eocene accretion in the northwestern U.S., rather than coherent post-Laramide rollback.

3.3.2. Lithospheric heterogeneity and instabilities

We find more complex structure within and near the base of the lithosphere (60–160 km) than continental (Bedle and Van der Lee, 2009) or global (Lebedev and van der Hilst, 2008) scale studies find using longer-period data from sparser networks that pre-date the TA. The most prominent difference in regional lithospheric structure is a southwest trending swath of high-velocity lithosphere extending from the central Colorado Plateau to northeastern Wyoming, with generally lower-velocity mantle beneath the adjacent SRP, Basin and Range, Colorado Rockies, and RGR (Fig. 4). This arm of high-velocity lithosphere crosses the continental divide in WY and underlies some of the highest topography in the western U.S. A smaller region of high-velocity lithosphere lies beneath western Idaho and easternmost Oregon and Washington, straddling the boundary between Precambrian continental lithosphere and the accreted oceanic terranes (Fig. 4). In the tectonically stable portion of the western U.S., high-velocity mantle underlies northern Montana and the western Great Plains south of Nebraska. Thus, strong mantle heterogeneity is being revealed beneath both tectonically active and tectonically quiescent domains of the western U.S.

Most of the Colorado Plateau is distinguished from the surrounding Basin and Range and RGR provinces by the presence of laterally continuous high-velocity mantle from 60 to 125 km depth (Fig. 4), and the Colorado Plateau–Great Basin transition is one of the strongest upper mantle velocity gradients in the western U.S. (Sine et al., 2008), we find up to 8% V_P and 14.5% V_S variations over <150 km. At these depths, however, the transition from Colorado Plateau to Basin and Range mantle often lies inboard of the Colorado Plateau margin. This is especially true of the southwestern plateau (including the Grand Canyon and San Francisco Peaks volcanic field). In addition, isolated, high-velocity volumes beneath southern Utah and northwestern New Mexico extend to depths of ~230 km and ~200 km, respectively (Fig. 4). Low seismic velocities beneath the margins of the Colorado Plateau, in conjunction with the elevated plateau rim and co-located geoid high (Karlstrom et al., 2008), frequent seismicity, and late-Cenozoic migration of volcanism onto the Colorado Plateau, suggest approximately concentric thermal erosion of a lithospheric step originally located beneath the topographic boundary of the Colorado Plateau (Karlstrom et al., 2008; Roy et al., 2009). The presence of the two deeper, drip-like high-velocity bodies and the absence of thick high-velocity mantle lithosphere beneath much of the southwestern Colorado Plateau indicate that more localized 3-D lithospheric downwelling also is

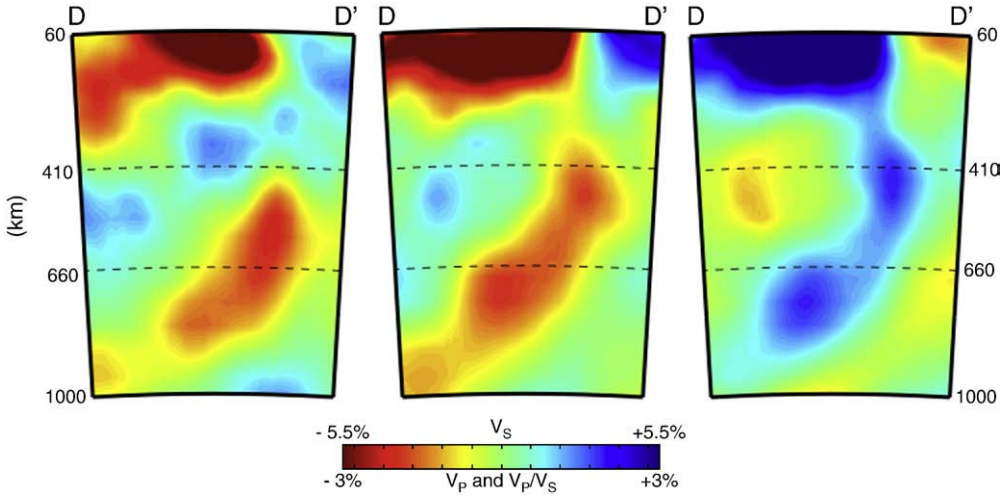

Fig. 8. Cross-section through the eastern SRP and Yellowstone. The location of the cross-section D–D′ is labeled in Fig. 4. All panels show the same section. Isolated V_P model (left), isolated V_S model (center), and V_P/V_S model from the joint inversion (right). Maximum perturbations are −4.75% V_P, −11% V_S, and +7% V_P/V_S at 60–90 km depth beneath Yellowstone and the easternmost SRP.

occurring, which may contribute importantly to the Cenozoic uplift of the plateau.

In several other areas, small-scale (100–200 km) high-velocity features extend to depths of 200–250 km, and often are surrounded by low-velocity, high V_P/V_S mantle (Fig. 4). The large magnitude and drip-like geometry of these anomalies lead us to infer that both 3-D gravitational instabilities and edge-driven convection are actively modifying the western U.S. lithosphere. Temperature contrast owing to lithospheric downwelling probably is the dominant cause of these anomalies. However, imaged large velocity reductions (with respect to the already low-velocity mean of western U.S. asthenosphere) and the expectation of ascending return flow suggest that partial melt may be present within the very low-velocity volumes. Small-scale upper mantle convection driven by the recent sinking of dense mafic roots of plutons has been proposed for the uplifted southern Sierra Nevada (Ducea and Saleeby, 1998; Zandt et al., 2004) and Wallowa Mountains (Hales et al., 2005), and oblique convergence at the "Big Bend" in the San Andreas fault is thought to drive downwelling of mantle lithosphere creating the high-velocity anomaly beneath the Transverse Ranges (Bird and Rosenstock, 1984; Humphreys and Hager, 1990). Edge convection driven by abrupt changes in lithospheric thickness has been proposed to explain mantle velocity contrasts at the edge of the Colorado plateau (Sine et al., 2008) and beneath the Rio Grande Rift–Great Plains transition (Gao et al., 2004; Song and Helmberger, 2007).

3.3.3. Snake River Plain–Yellowstone hotspot

The most prominent low-velocity, high V_P/V_S anomaly occupies the ~200 km beneath Yellowstone and the eastern SRP (Figs. 4 and 8). A broader, lower magnitude low-velocity, high V_P/V_S anomaly occupies the transition zone and extends to ~900 km beneath the Yellowstone region. It appears separate from the shallow anomaly in the V_P model and weakly connected in the V_S and V_P/V_S models (Fig. 8). The deeper low-velocity volume extends just to the bottom of what we consider the well-resolved model domain (885 km). It is worth noting that the anomaly is not present in the bottom two layers of the entire model. If a low-velocity conduit extended to greater depth than the base of our model (1015 km), we would expect a large velocity anomaly to accumulate in the deepest layers. In agreement with other recent studies (Yuan and Dueker, 2005; Sigloch et al., 2008; Burdick et al., 2009; Tian et al., 2009; Smith et al., 2009, Xue and Allen, in press), we do not find a strong low-velocity conduit that extends continuously into the lower mantle. The proximity of major high-velocity bodies suggests mantle ascent beneath Yellowstone is driven by sinking cool masses as well as its own positive buoyancy (Fig. 6). The ~12 m geoid high centered on Yellowstone indicates that the Yellowstone topographic swell is compensated at depths greater than the rest of elevated western U.S. (Lowry et al., 2000), which is attributed to buoyancy of the very low-velocity mantle imaged in the upper 200 km.

4. Conclusions

We provide a new level of constraint on 3-D seismic heterogeneity and the distribution of partial melt in the western U.S. upper mantle. The seismic structure presented here and the spatial and temporal distribution of volcanic and tectonic activity in the western U.S. indicate a complex syn- and post-Laramide subduction history and currently active widespread small-scale convection. It remains a challenge to understand specifically all the events that lead to segmentation subducted Farallon slab and how those events relate to surface geologic activity. At present, a diverse range of small-scale convective processes appear to be active beneath the western U.S. including 3-D lithospheric drips, edge-driven convection, and an upper mantle plume, but further constraints on upper mantle physical state are necessary to determine the conditions that drive this spectrum of activity. Additionally, it is unclear how the provincially heterogeneous lithosphere we image supports the elevation of the western U.S. plateau, and we place particular emphasis on a need to understand the buoyancy structure of the high-velocity lithosphere that apparently underlies much of the high topography of Wyoming and the Colorado Plateau. Progress in these directions will require knowledge of 3-D attenuation structure and careful integration of body-waves, surface-waves, and receiver functions to achieve shorter wavelength resolution of mantle structure.

Acknowledgements

Seismic data were acquired from the IRIS DMC, SCEDC, NCEDC, and CNDC. We thank the scores of investigators who collected the seismic data used in this study and those who have worked to archive and distribute these data. We thank the principal investigators responsible for the SNEP, CAFE, HLP, and SIEDCAR arrays for graciously sharing their data. Thoughtful comments from two anonymous helped improve the manuscript. This work was supported by NSF grants EAR 952194, EAR 911006, EAR 745899, EAR 511000, and benefited from computational facilities provided by EAR 065123.

Appendix A. Supplementary data

Supplementary data associated with this article can be found, in the online version, at doi:10.1016/j.epsl.2010.06.047.

References

Anderson, O.L., Isaak, D., Oda, H., 1992. High-temperature elastic constant data on minerals relevant to geophysics. Rev. Geophys. 30, 57–90.

Atwater, T., 1970. Implications of plate tectonics for Cenozoic tectonic evolution of western North America. Geol. Soc. Am. Bull. 81, 3513–3536.

Bedle, H., Van der Lee, S., 2009. S velocity variations beneath North America. J. Geophys. Res. 114, B07308. doi:10.1029/2008JB005949.

Bird, P., 1979. Continental delamination and the Colorado Plateau. J. Geophys. Res. 84, 7561–7571.

Bird, P., 1984. Laramide crustal thickening event in the rocky mountain foreland and great plains. Tectonics 3, 741–758.

Bird, P., Rosenstock, R.W., 1984. Kinematics of present crust and mantle flow in southern California. Geol. Soc. Am. Bull. 95, 946–957.

Bunge, H.-P., Grand, S., 2000. Mesozoic plate-motion history below the northeast Pacific Ocean from seismic images of the subducted Farallon slab. Nature 405, 337–340.

Burchfiel, B.C., Cowen, D.S., Davis, G.A., 1992. Tectonic overview of the Cordilleran orogen in the western U.S. In: Burchfiel, B.C., Lipman, P., Zoback, M.L. (Eds.), The Geology of North America: The Cordilleran Orogen: Conterminous U.S, G-3. Geological Society of America, Boulder, Colololorado, pp. 407–479.

Burdick, S., et al., 2009. Model update December 2008: upper mantle heterogeneity beneath North America from P-wave travel time tomography with global and USArray transportable array data. Seismol. Res. Lett. 80 (4), 638–645.

Carlson, R.W., Hart, W.K., 1987. Crustal genesis on the Oregon Plateau. J. Geophys. Res. 92 (B7), 6191–6206. doi:10.1029/JB092iB07p06191.

Christiansen, R.L., Yeats, R.S., 1992. Post-Laramide geology of the western U.S. Cordillera. In: Burchfiel, B.C., Lipman, P., Zoback, M.L. (Eds.), The Geology of North America: The Cordilleran Orogen: Conterminous U.S, G-3. Geological Society of America, Boulder, Colololorado, pp. 261–406.

Chulick, G.S., Mooney, W.D., 2002. Seismic structure of the crust and uppermost mantle of North America and adjacent oceanic basins: a synthesis. Bull. Seismol. Soc. Am. 92 (6), 2478–2492.

Coney, P.J., Harms, T.A., 1984. Cordilleran metamorphic core complexes: Cenozoic extensional relics of Mesozoic compression. Geology 12, 550–554.

Coney, P.J., Reynolds, S.J., 1977. Flattening of the Farallon slab. Nature 270, 403–406.

Dahlen, F.A., Hung, S.-H., Nolet, G., 2000. Frechet kernels for finite-frequency traveltimes, I. Theory Geophys. J. Int. 141, 157–174.

Dalton, C.A., Ekstrom, G., Dziewonski, A.M., 2008. The global attenuation structure of the upper mantle. J. Geophys. Res. 113, B09303. doi:10.1029/2007JB005429.

DeCelles, P.G., 2004. Late Jurassic to Eocene evolution of the Cordilleran thrust belt and foreland basin system, western U.S.A. Am. J. Sci. Vol. 304, 105–168. doi:10.2475/ajs.304.2.105.

Dickinson, W.R., Snyder, W.S., 1979. Geometry of subducted slabs related to the San Andreas transform. J. Geol. 87, 609–627.

Dixon, J.E., Dixon, T.H., Bell, D.R., Malservisi, R., 2004. Lateral variation in upper mantle viscosity: role of water. Earth Planet. Sci. Lett. 222, 451–467.

Ducea, M., Saleeby, J., 1998. A case for delamination of the deep batholithic crust beneath the Sierra Nevada. California Int. Geol. Rev. 40, 78–93.

Engebretsen, D.C., Cox, A., Gordon, R.G., 1985. Relative motions between oceanic and continental plates in the Pacific Basin. Geol. Soc. Am. 206, 560–569 Spec. Pap.

Gao, W., et al., 2004. Upper mantle convection beneath the central Rio Grande rift imaged by P and S wave tomography. J. Geophys. Res. 109, B03305. doi:10.1029/2003JB002743.

Gaschnig, R.M., Vervoort, J.D., Lewis, R.S., McClelland, W.C., 2009. Migrating magmatism in the northern US Cordillera: in situ U–Pb geochronology of the Idaho batholith. Contrib Mineral Petrol. DOI. doi:10.1007/s00410-009-0459-5.

Gilbert, H.J., Fouch, M., 2007. Complex upper mantle seismic structure across the southern Colorado Plateau/Basin and Range II: results from receiver function analysis. Eos Trans. AGU 88, S41B-0558.

Goes, S., Van der Lee, S., 2002. Thermal structure of the North American uppermost mantle inferred from seismic tomography. J. Geophys. Res. 107 (B3), 2050. doi:10.1029/2000JB000049.

Goes, S., Govers, R., Vacher, P., 2000. Shallow mantle temperatures under Europe from P and S wave tomography. J. Geophys. Res. 105, 11,153–11,170.

Golombek, M.P., McGill, G.E., Brown, L., 1983. Tectonic and geologic evolution of the Española Basin, Rio Grande rift: structure, rate of extension, and relation to the state of stress in the Western US. Tectonophysics 94, 483–507.

Grand, S.P., 1994. Mantle shear structure beneath the Americas and surrounding oceans. J. Geophys. Res. 99, 11,591–11,621.

Gripp, A.E., Gordon, R.G., 2002. Young tracks of hotspots and current plate velocities. Geophys. J. Int. 150, 321–361.

Hales, T.C., Abt, D.L., Humphreys, E.D., Roering, J.J., 2005. A lithospheric instability origin for Columbia River flood basalts and Wallowa Mountains uplift in northeast Oregon. Nature 438, 842–845. doi:10.1038/nature04313.

Hammond, W.C., Humphreys, E.D., 2000. Upper mantle seismic wave velocity: effects of realistic partial melt geometries. J. Geophys. Res. 105 (B5), 975–986.

Hammond, W.C., Toomey, D.R., 2003. Seismic velocity anisotropy and heterogeneity beneath the Mantle Electromagnetic and Tomography Experiment (MELT) region of the East Pacific Rise from analysis of P and S body waves. J. Geophys. Res. 108 (B4), 2176. doi:10.1029/2002JB001789.

Heller, P.L., Dueker, K., McMillan, M., 2003. Post-Paleozoic alluvial gravel transport as evidence of continental tilting in the Cordilleran, United States. Geol. Soc. Am. Bull. 115, 1122–1132.

Hirschmann, M.M., 2006. Water, melting, and the deep earth H_2O cycle. Annu. Rev. Earth Planet. Sci. 34, 629–653. doi:10.1146/annurev. earth.34.031405.125211.

Humphreys, E.D., 1995. Post-Laramide removal of the Farallon slab, western United States. Geology 23, 987–990.

Humphreys, E.D., 2009. Cenozoic slab windows beneath the western U.S. In: Spencer, J.E., Titley, S. (Eds.), Circum-Pacific Tectonics, Geologic Evolution, and Ore Deposits Cenozoic, 22. Arizona Geological Society Digest, pp. 389–396.

Humphreys, E.D., Dueker, K., 1994. Western US upper mantle structure. J. Geophys. Res. 99, 9615–9634.

Humphreys, E.D., Hager, B.H., 1990. A kinematic model for the late Cenozoic development of southern California crust and upper mantle. J. Geophys. Res. 95, 19,747–19,762.

Humphreys, E.D., et al., 2003. How Laramide-age hydration of North American lithosphere by the Farallon slab controlled subsequent activity in the western. U.S. Int. Geol. Rev. 45, 575–595.

Jacobsen, S.D., et al., 2008. Effects of hydration on the elastic properties of olivine. Geophys. Res. Lett. 35, L14303. doi:10.1029/2008GL034398.

Karato, S., 1993. Importance of anelasticity in the interpretation of seismic tomography. Geophys. Res. Lett. 20, 1623–1626.

Karlstrom, K.E., Crow, R., Crossey, L.J., Coblentz, D., Van Wijk, J.W., 2008. Model for tectonically driven incision of the younger than 6 Ma Grand Canyon. Geology 36, 835–838. doi:10.1130/G25032A.1.

Kennett, B.L.N., Engdahl, E.R., Buland, R., 1995. Constraints on seismic velocities in the Earth from travel times. Geophys. J. Int. 122, 108–124.

Lebedev, S., van der Hilst, R., 2008. Global upper mantle tomography with the automated inversion of surface and S-waveforms. Geophys. J. Int. 173, 505–518. doi:10.1111/j.1365-246X.2008.03721.x.

Lee, C.-T.A., 2003. Compositional variation of density and seismic velocities in natural peridotites at STP conditions: implications for seismic imaging of compositional heterogeneities in the upper mantle. J. Geophys. Res. 108 (B9), 2441. doi:10.1029/2003JB002413.

Li, X., Yuan, X., Kind, R., 2007. The lithosphere–asthenosphere boundary beneath the western United States. Geophys. J. Int. 170 (2), 700–710.

Lin, F.-C., Moschetti, M.P., Ritzwoller, M.H., 2008. Surface wave tomography of the western United States from ambient seismic noise: Rayleigh and Love wave phase velocity maps. Geophys. J. Int. 173, 281–298. doi:10.1111/j.1365-246X.2008.03720.x.

Lithgow-Bertelloni, C., Richards, M.A., 1998. The dynamics of Cenozoic and Mesozoic plate motions. Rev. Geophys. 36, 27–78.

Livaccari, R.F., Burke, K., Sengor, A.M.C., 1981. Was the Laramide orogeny related to subduction of an oceanic plateau. Nature v. 289, 276–278.

Lowry, A.R., Ribe, N.M., Smith, R.B., 2000. Dynamic elevation of the Cordillera, western United States. J. Geophys. Res. 105 (B10), 23,371–23,390.

Madsen, J.K., Thorkelson, D.J., Friedman, R.M., Marshall, D.D., 2006. Cenozoic to Recent plate configurations in the Pacific Basin: Ridge subduction and slab window magmatism in western North America. Geosphere. 2, 11–34.

Muller, R.D., Sdrolias, M., Gaina, G., Roest, W.R., 2008. Age, spreading rates, and spreading asymmetry of the world's ocean crust. Geochem. Geophys. Geosys. 9, Q04006. doi:10.1029/2007GC001743.

Piromallo, C., Becker, T.W., Funiciello, F., Faccenna, C., 2006. Three-dimensional instantaneous mantle flow induced by subduction. Geophys. Res. Lett. 33, L08304. doi:10.1029/2005GL025390.

Pollitz, F.F., Snoke, J.A., 2010. Rayleigh-wave phase-velocity maps and three-dimensional shear velocity structure of the western US from local non-plane surface wave tomography. Geophys. J. Int. 180, 1153–1169.

Reiners, P.W., et al., 2002. Late Miocene exhumation and uplift of the Washington Cascades. Geology 30, 767–770.

Riihimaki, C.A., Anderson, R.S., Safran, E.B., 2007. Impact of rock uplift on rates of late Cenozoic Rocky Mountain river incision. J. Geophys. Res. 112, F03S02. doi:10.1029/2006JF000557.

Ritsema, J., van Heijst, H.J., Woodhouse, J., Deuss, A., 2009. Long-period body-wave traveltimes through the crust: implication for crustal corrections and seismic tomography. Geophys. J. Int. 179 (2), 1255–1261.

Romanowicz, B., 1979. Seismic structure of the upper mantle beneath the United States by three dimensional inversion of body wave arrival times. Geophys. J. R. astr. Soc. 57, 479–506.

Romanowicz, B., Cara, M., 1980. Reconsideration of the relations between P and S station anomalies in North America. Geophys. Res. Lett. 7, 417–420.

Roth, J.B., Fouch, M.J., James, D.E., Carlson, R.W., 2008. Three-dimensional seismic velocity structure of the northwestern United States. Geophys. Res. Lett. 35, L15304.

Roy, M., Jordan, T.H., Pederson, J., 2009. Colorado Plateau magmatism and uplift by warming of heterogeneous lithosphere. Nature 459, 978–982.

Saleeby, J., 2003. Segmentation of the Laramide Slab — evidence from the southern Sierra Neveda region. Bull. Geol. Soc. Am. 115, 655–668.

Schmandt, B., Humphreys, E.D., 2010. Seismic heterogeneity and small-scale convection in the southern California upper mantle. Geochem. Geophys. Geosys. 11, Q05004. doi:10.1029/2010GC003042.

Schutt, D.L., Lesher, C.E., 2006. Effects of melt depletion on the density and seismic velocity of garnet and spinel lherzolite. J. Geophys. Res. 111, B05401. doi:10.1029/2003JB002950.

Schutt, D.L., Dueker, K., 2008. Temperature of the plume layer beneath the Yellowstone hotspot. Geology 36 (8), 623–626. doi:10.1130/G24809A.

Sigloch, K., McQuarrie, N., Nolet, G., 2008. Two-stage subduction history under North America inferred from multiple-frequency tomography. Nat. Geosci. 1, 458–462.
Sine, C.R., et al., 2008. Mantle structure beneath the western edge of the Colorado Plateau. Geophys. Res. Lett. 35. doi:10.1029/2008GL033391.
Smith, R.B., et al., 2009. Geodynamics of the Yellowstone hotspot and mantle plume: seismic and GPS imaging, kinematics, and mantle flow. J. Volcanol. Geotherm. Res. 188, 26–56. doi:10.1016/j.jvolgeores.2009.08.020.
Song, T.-R.A., Helmberger, D.V., 2007. P and S waveform modeling of continental sub-lithospheric detachment at the eastern edge of the Rio Grande Rift. J. Geophys. Res. 112, B07319. doi:10.1029/2007JB004942.
Spencer, J.E., 1996. Uplift of the Colorado Plateau due to lithosphere attenuation during Laramide low-angle subduction. J. Geophys. Res. 101, 13,595–13,609.
Stachnik, J.C., Dueker, K., Schutt, D.L., Yuan, H., 2008. Imaging Yellowstone plume–lithosphere interactions from inversion of ballistic and diffusive Rayleigh wave dispersion and crustal thickness data. Geochem. Geophys. Geosyst. 9, Q06004. doi:10.1029/2008GC001992.
Stock, J., Molnar, P., 1988. Uncertainties and implications of the Late Cretaceous and Tertiary position of North America relative to the Farallon, Kula, and Pacific plates. Tectonics 7, 1339–1384.
Tape, C., Liu, Q., Maggi, A., Tromp, J., 2009. Adjoint tomography of the southern California crust. Science 325, 988. doi:10.1126/science.1175298.
Thurber, C., Zhang, H., Brocher, T., Langenheim, V., 2009. Regional three-dimensional seismic velocity model of the crust and uppermost mantle of northern California. J. Geophys. Res. 114, B01304. doi:10.1029/2008JB005766.
Tian, Y., Sigloch, K., Nolet, G., 2009. Multiple-frequency SH-wave tomography of the western US upper mantle. Geophys. J. Int. 178 (3), 1384–1402. doi:10.1111/j.1365-246X.2009.04225.x.
VanDecar, J.C., Crosson, R.S., 1990. Determination of teleseismic relative phase arrival times using multi-channel cross-correlation and least squares. Bull. Seismol. Soc. Am. 80, 150–169.
West, J.D., Fouch, M.J., Roth, J.B., Elkins-Tanton, L.T., 2009. Vertical mantle flow associated with a lithospheric drip beneath the Great Basin. Nat. Geosci. 2, 439–444.
Xue, M. and R. M. Allen, 2010. Mantle structure beneath the western United States and its implications for convection processes. J. Geophys. Res., doi:10.1029/2008JB006079, in press.
Yang, Y., Forsyth, D.W., 2008. Attenuation in the upper mantle beneath Southern California: physical state of the lithosphere and asthenosphere. J. Geophys. Res. 113, B03308. doi:10.1029/2007JB005118.
Yang, Y., Ritzwoller, M.H., Lin, F.-C., Moschetti, M.P., Shapiro, N.M., 2008. Structure of the crust and uppermost mantle beneath the western United States revealed by ambient noise and earthquake tomography. J. Geophys. Res. 113, B12310. doi:10.1029/2008JB005833.
Yuan, H., Dueker, K., 2005. Teleseismic P-wave tomogram of the Yellowstone plume. Geophys. Res. Lett. 32, L07304. doi:10.1029/2004GL022056.
Zandt, G., Humphreys, E.D., 2008. Toroidal through the western U.S. slab window. Geology 36, 295–298.
Zandt, G., et al., 2004. Active foundering of a continental arc root beneath the southern Sierra Nevada in California. Nature 431, 41–46.